

RESEARCH

Open Access



Baicalin-loaded folic acid-modified albumin nanoparticles (FA-BSANPs/BA) induce autophagy in MCF-7 cells via ROS-mediated p38 MAPK and Akt/mTOR pathway

Fengjie Liu^{1†}, Meng Lan^{1†}, Baoqi Ren^{2†}, Lihong Li¹, Tengteng Zou¹, Zhaodi Kong¹, Dongmei Fan^{3*}, Tiange Cai^{4*} and Yu Cai^{1,5*} 

*Correspondence:
dongmeifan9@sina.com;
caitiange@163.com;
caiyu@sohu.com

[†]Fengjie Liu, Meng Lan and Baoqi Ren contributed equally to this work

¹ College of Pharmacy,
Jinan University,
Guangzhou 510632,
Guangdong, China

³ Department
of Gastroenterology,
First Affiliated Hospital
of Guangzhou University
of Chinese Medicine,
Guangzhou 510405,
Guangdong, China

⁴ College of Life Sciences,
Liaoning University,
Shenyang 110036, Liaoning,
China

Full list of author information
is available at the end of the
article

Abstract

Background: Breast cancer is the most frequently occurring cancer among women. Baicalin has been shown to inhibit breast cancer proliferation, but poor aqueous solubility and unknown mechanism of action limit its application. This study aimed to investigate the antiproliferative effects of baicalin-loaded folic acid-modified albumin nanoparticles (FA-BSANPs/BA) in breast cancer MCF-7 cells and its relationship with autophagy and ROS-mediated p38 MAPK and Akt/mTOR signaling pathways. Cell viability was detected by MTT assay. Flow cytometry and fluorescence microscopy were used to detect cell cycle, apoptosis and autophagy. Western blot was used to detect protein expression.

Results: Compared with the control and free baicalin groups, FA-BSANPs/BA inhibited viability of MCF-7 cells and increased cells in S phase, apoptotic bodies, pro-apoptotic proteins, autophagy markers and autophagosomes. These effects could be reversed when combined with the autophagy inhibitor 3-methyladenine. FA-BSANPs/BA increased the levels of phosphorylated p38 MAPK, inhibited the levels of phosphorylated Akt and mTOR, and increased the level of ROS in MCF-7 cells. The effects of FA-BSANPs/BA could be reversed or enhanced using inhibitors of Akt, mTOR, p38 MAPK and ROS scavengers.

Conclusions: Encapsulation in folate albumin nanoparticles improved the antiproliferative activity of baicalin. FA-BSANPs/BA induced autophagy and apoptosis via ROS-mediated p38 MAPK and Akt/mTOR signaling pathways in human breast cancer cells.

Keywords: Baicalin, Albumin nanoparticles, Breast cancer, Autophagy, Signal pathway

Introduction

Breast cancer (BC) remains the most prevalent cancer among women, accounting for 22.9% of all cancers in women (De Cicco et al. 2019; Siegel et al. 2020). Chemotherapy is an important approach for the treatment of BC. However, traditional chemotherapeutic drugs are often accompanied by side effects and eventually suffer from



© The Author(s), 2022. **Open Access** This article is licensed under a Creative Commons Attribution 4.0 International License, which permits use, sharing, adaptation, distribution and reproduction in any medium or format, as long as you give appropriate credit to the original author(s) and the source, provide a link to the Creative Commons licence, and indicate if changes were made. The images or other third party material in this article are included in the article's Creative Commons licence, unless indicated otherwise in a credit line to the material. If material is not included in the article's Creative Commons licence and your intended use is not permitted by statutory regulation or exceeds the permitted use, you will need to obtain permission directly from the copyright holder. To view a copy of this licence, visit <http://creativecommons.org/licenses/by/4.0/>. The Creative Commons Public Domain Dedication waiver (<http://creativecommons.org/publicdomain/zero/1.0/>) applies to the data made available in this article, unless otherwise stated in a credit line to the data.

reduced efficacy due to the acquisition of tumor drug resistance (Waks and Winer 2019). Baicalin (BA) is a flavonoid that can be isolated from the roots of *Scutellaria baicalensis Georgi* (Li-Weber 2009). Over the past 30 years, it has been shown to have antiproliferative activity against certain cancers, including BC, liver cancer, and ovarian cancer, by inducing apoptosis, blocking the cell cycle, triggering autophagy, and inhibiting angiogenesis (Gao et al. 2017; Zhou et al. 2009; Peng et al. 2015; Zhu et al. 2018). However, the lower aqueous solubility of BA may hinder its clinical translation (Ahmed et al. 2020). Albumin nanocarriers, which can improve the biocompatibility of drugs, prolong the circulation time in vivo, and easily enhance the aggregation of drugs at the tumor site through targeting ligand modification, are considered to be an effective strategy to help antitumor drugs move to the market (Tao et al. 2019; Bhushan et al. 2017). Drugs have been successfully developed using folic acid (FA)-modified albumin nanoparticles as carriers, such as paclitaxel (Zhao et al. 2010), mitoxantrone (Zhang et al. 2010), doxorubicin (Shen et al. 2011), resveratrol (Lian et al. 2019), and others.

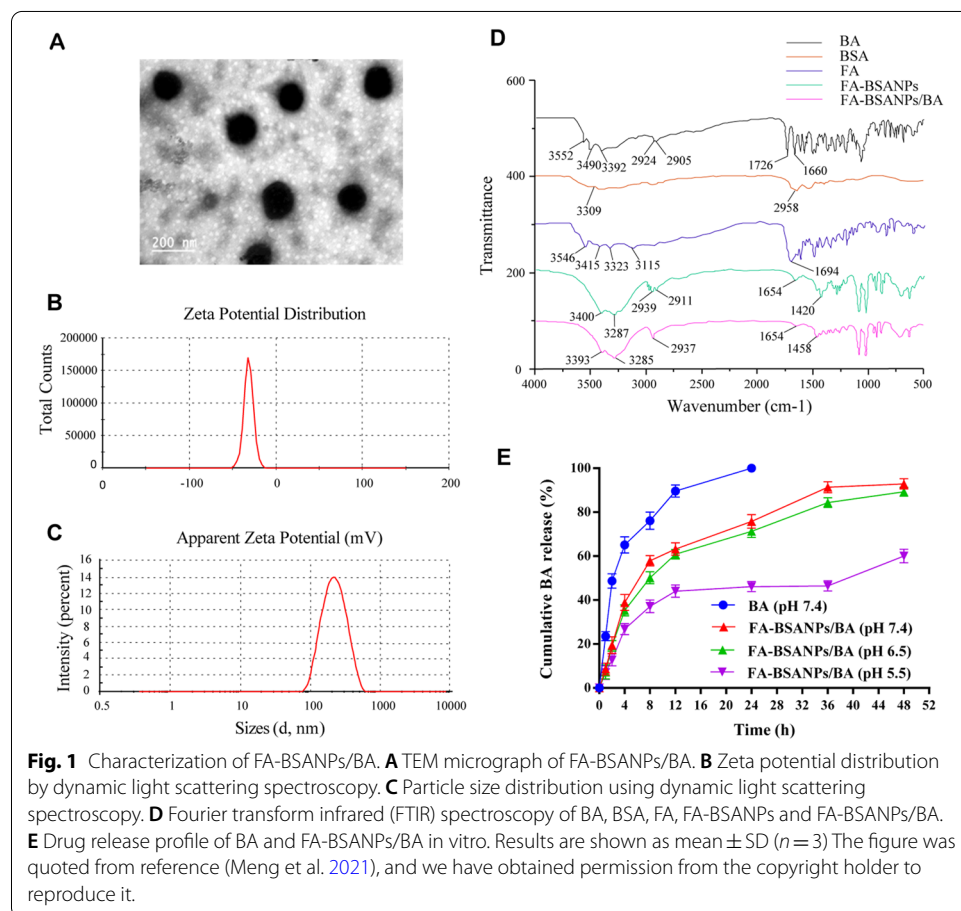
The process of tumor initiation and progression is often accompanied by a disturbance in the function of apoptosis (Carneiro and El-Deiry 2020). Autophagy is essential for the regulation of cellular homeostasis under stressful circumstances such as the tumor microenvironment (Mancias and Kimmelman 2016). At the early stage of tumor formation, autophagy synergizes with apoptosis to suppress tumor development by degrading and restoring captured proteins and organelles, whereas at the late stage of tumor development, autophagy may also serve as a protective mechanism to provide nutrients to tumor cells and inhibit apoptosis (Zhang et al. 2012). Recent studies found that BA induced autophagy and reduced cancer cell proliferation by downregulating autophagy markers microtubule-associated protein 1 light chain 3 (LC3)-I, LC3-II, Beclin-1, autophagy-related 12 (Atg12), Atg7, Atg5 and upregulating adenosine monophosphate (AMP)-activated protein kinase (AMPK) signaling (Singh et al. 2021). However, the molecular mechanism linking the effect of BA in inhibiting BC cell proliferation and autophagy needs further investigation. Excessive reactive oxygen species (ROS) are known to cause oxidative stress and metabolic abnormalities, leading to organelle damage, which can trigger autophagy and apoptosis (Trachootham et al. 2009; Yang and Lian 2020). The interplay between ROS-mediated apoptosis and autophagy involves several signal pathways, including c-Jun N-terminal kinase (JNK), extracellular signal-regulated kinase (p38 MAPK), mitogen-activated protein kinase (ERK), and V-akt murine thymoma viral oncogene homolog (AKT)/mammalian target of rapamycin (mTOR) (Moloney and Cotter 2018; Sui et al. 2014; Prasad et al. 2017). ROS-mediated signaling pathways are potential molecular mechanisms by which BA affects autophagy in BC.

In this study, we constructed BA-loaded folic acid-modified albumin nanoparticles (FA-BSANPs/BA) and demonstrated that the antiproliferative effect of FA-BSANPs/BA on BC MCF-7 cells was associated with the induction of cell cycle arrest, apoptosis and autophagy. Through the detection of ROS level, signal pathway protein activity and the use of inhibitors in MCF-7 cells, we further proved the intervention effect of FA-BSANPs/BA in ROS-mediated p38 MAPK and Akt/mTOR pathways, which provided new evidence for its antiproliferation mechanism.

Table 1 Characterization of FA-BSANPs and FA-BSANPs/BA

Detection items	FA-BSANPs	FA-BSANPs/BA
Particle size (nm)	183.41 ± 2.65	228.41 ± 2.36
Polydispersity index (PDI)	0.184 ± 0.03	0.264 ± 0.06
Zeta potential (mV)	-30.32 ± 2.43	-32.70 ± 1.27
Encapsulation efficiency (%)	—	76.88 ± 0.59
Drug loading (%)	—	7.41 ± 0.23
Folate coupling efficiency ($\mu\text{g}/\text{mg}$ BSA)	73.09 ± 2.46	66.45 ± 1.78

The data were quoted from reference (Meng et al. 2021), and we have obtained permission from the copyright holder to reproduce it.



Results

Characterization of FA-BSANPs/BA

Partial physicochemical properties of the prepared and optimized nanoformulations were examined, and these results are shown in Fig. 1A–D. The transmission electron microscopy (TEM) micrograph of optimized FA-BSANPs/BA showed smooth spheres. The particle size, zeta-potential, encapsulation efficiency and drug loading of FA-BSANPs/BA are shown in Table 1, which characterize them as small particle size with narrow distribution range and good polydispersity. The Fourier transform infrared (FTIR) spectroscopy of FA, BSA, BA, FA-BSANPs and FA-BSANPs/BA showed that

FA-BSANPs and FA-BSANPs/BA had the characteristic absorption peak of amide bond in BSA at 1654 cm^{-1} and the characteristic absorption peak of benzene ring in FA at 1458 cm^{-1} , and that FA-BSANPs/BA had the characteristic absorption peak of phenolic hydroxyl group in BA at 3393 cm^{-1} , indicating that BA was introduced into the conjugates of FA with albumin.

In vitro drug release

As shown in Fig. 1E, the results of in vitro drug release showed 100% release rate of free BA after 24 h, while only 91.34% of BA in FA-BSANPs/BA was released after 36 h (Meng et al. 2021). In the medium with pH of 7.4, 6.5 and 5.5, the release rates of BA from FA-BSANPs/BA after 48 h were 92.86, 97.23 and 60.05%, respectively. The release behavior of the preparation showed the characteristics of fast release in the early stage of the test and slow release in the late stage of the test, which may be due to the fact that most BA is encapsulated in the nanoparticles. In addition, although the preparation was not uniquely functionally modified, the release of the drug showed pH dependence, which was manifested by less release under more acidic conditions at the same time. However, the difference in drug release rates between pH 7.4 and 6.5 (considered to be in the acidity range of the tumor microenvironment) was not significant ($p > 0.05$). The mechanisms underlying these behaviors require further investigation.

To better describe the release behavior of FA-BSANPs/BA, we fitted the cumulative release profiles of BA and FA-BSANPs/BA with the zero-level equation, first-level equation and Higuchi equation mathematical models. The results are shown in Table 2. The previous results (Meng et al. 2021) and the added experiments showed that the release of the drug was best fitted by the first-order equation. The certain sustained-release behavior will help to keep the drug in the nanoparticles for a long time before reaching tumor site, improve the accumulation of the drug at the tumor site, and reduce the toxic side effects of the drug. More obvious tumor microenvironment pH-dependent drug release would be a target for future improvement.

Cellular uptake

Effective drug delivery should maximize the uptake of tumor cells and reduce the uptake of mononuclear phagocytic system. To evaluate this, the uptake of Coumarin-6

Table 2 Kinetic equations of BA release from FA-BSANPs/BA

pH of release medium	Fitting curve	Regression equation	R^2
7.4 [#]	First-order equation	$Mt = 89.14(1 - e^{-0.12t})$	0.98184
6.5	Zero-order equation	$Mt = 1.55t + 26.01$	0.79138
	First-order equation	$Mt = 84.78(1 - e^{-0.11t})$	0.97805
	Higuchi equation	$Mt = 13.29t^{0.5} + 4.79$	0.93049
	Zero-order equation	$Mt = 0.89t + 19.99$	0.68458
5.5	First-order equation	$Mt = 51.59(1 - e^{-0.15t})$	0.93788
	Higuchi equation	$Mt = 7.74t^{0.5} + 7.43$	0.83477

Mt: cumulative release rate of drug (%)

t time (h)

[#] Data of pH7.4 were quoted from reference (Meng et al. 2021), and we have obtained permission from the copyright holder to reproduce it

(C6)-labeled FA-BSANPs (FA-BSANPs/C6) and BSANPs (BSANPs/C6) in MCF-7 cells (Meng et al. 2021) and macrophages was observed by fluorescence imaging and flow cytometry. Representative images of macrophage uptake are shown in Fig. 2B. The mean fluorescence intensity of fluorescence-positive cells is shown in Fig. 2C. The intracellular fluorescence intensity of FA-BSANPs/C6 group was found significantly higher than that of BSANPs/C6 group and free C6 group in both MCF-7 cells and macrophages. In two kinds of cells, the mean fluorescence intensity of FA-BSANPs/C6 group was significantly stronger than that of BSANPs/C6 group and free C6 group; after the addition of free FA to compete with the nanoparticles, the intracellular fluorescence intensity of FA-BSANPs/C6 group decreased significantly. These results show that FA modification can improve the targeting ability of nanoparticles, significantly increase cell uptake and achieve intracellular drug delivery.

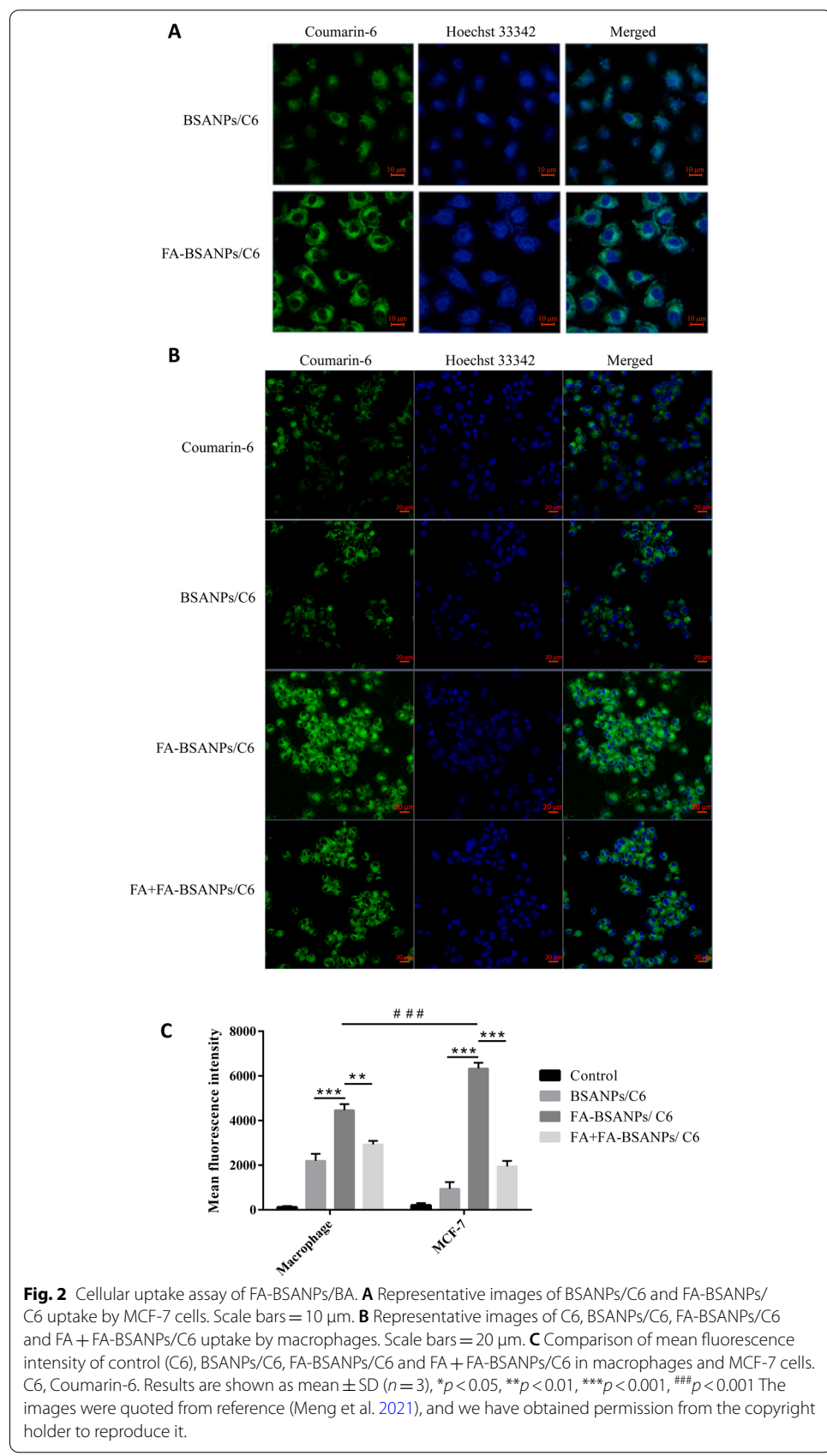
The results showed that macrophages could uptake the nanoparticles, and higher uptake of FA-modified nanoparticles was observed. This is presumed to be due to expression of folate receptors on activated macrophages. We examined the uptake of FA-BSANPs/C6 by MCF-7 cells previously and the results are shown in Fig. 2A and C. However, the mean fluorescence intensity was significantly greater in tumor cells than in macrophages (Fig. 2C) under the conditions that the drug concentration, treatment time, seeding and counting cell amount were kept the same as possible. This may lead to partial clearance of the nanoparticles by the mononuclear phagocytic system, but therapeutically, perhaps could be used to simultaneously target the large number of tumor-associated macrophages infiltrating the tumor site.

Biodistribution

To better evaluate the targeting effect and toxic side effects of the nanoparticles, MCF-7 tumor-bearing BALB/c nude mice were injected with indocyanine green (ICG)—loaded FA-BSANPs (FA-BSANPs/ICG). Representative near-infrared fluorescence images are shown in Additional file 1: Fig. S1. The results of near-infrared fluorescence imaging showed that FA-BSANPs/ICG were mainly distributed in tumor, liver and kidney tissues, and fluorescence appeared at the tumor site from 1 h after injection and could be maintained for 24 h, while ICG mice had no fluorescence signal at the tumor site. This confirmed the in vitro results, indicating that the nanoparticles had good tumor targeting. Modification strategies for improvement should be considered for evading clearance from the circulatory system and reducing toxic side effects of nanoparticles.

FA-BSANPs/BA induced cell cycle arrest and apoptosis in MCF-7 cells

MCF-7 cells were treated with FA-BSANPs, free BA and FA-BSANPs/BA at different concentrations (3.5, 7, 14, 28, 56, 112, 224, 448 μ M) for 24, 48, 72 h. MTT assay was used to detect viability of MCF-7 cells. It was found that administration of FA-BSANPs in the concentration range of 3.5~448 μ M did not decrease the proportion of surviving cells below 80%, while free BA and FA-BSANPs/BA decreased cell viability in a dose- and time-dependent manner (Fig. 3A). Data analysis showed that IC₅₀ values of FA-BSANPs/BA and BA were, respectively, 39.3 and 170 μ M, indicating that FA-BSANPs/BA possessed enhanced cytotoxicity compared to free BA. Low,



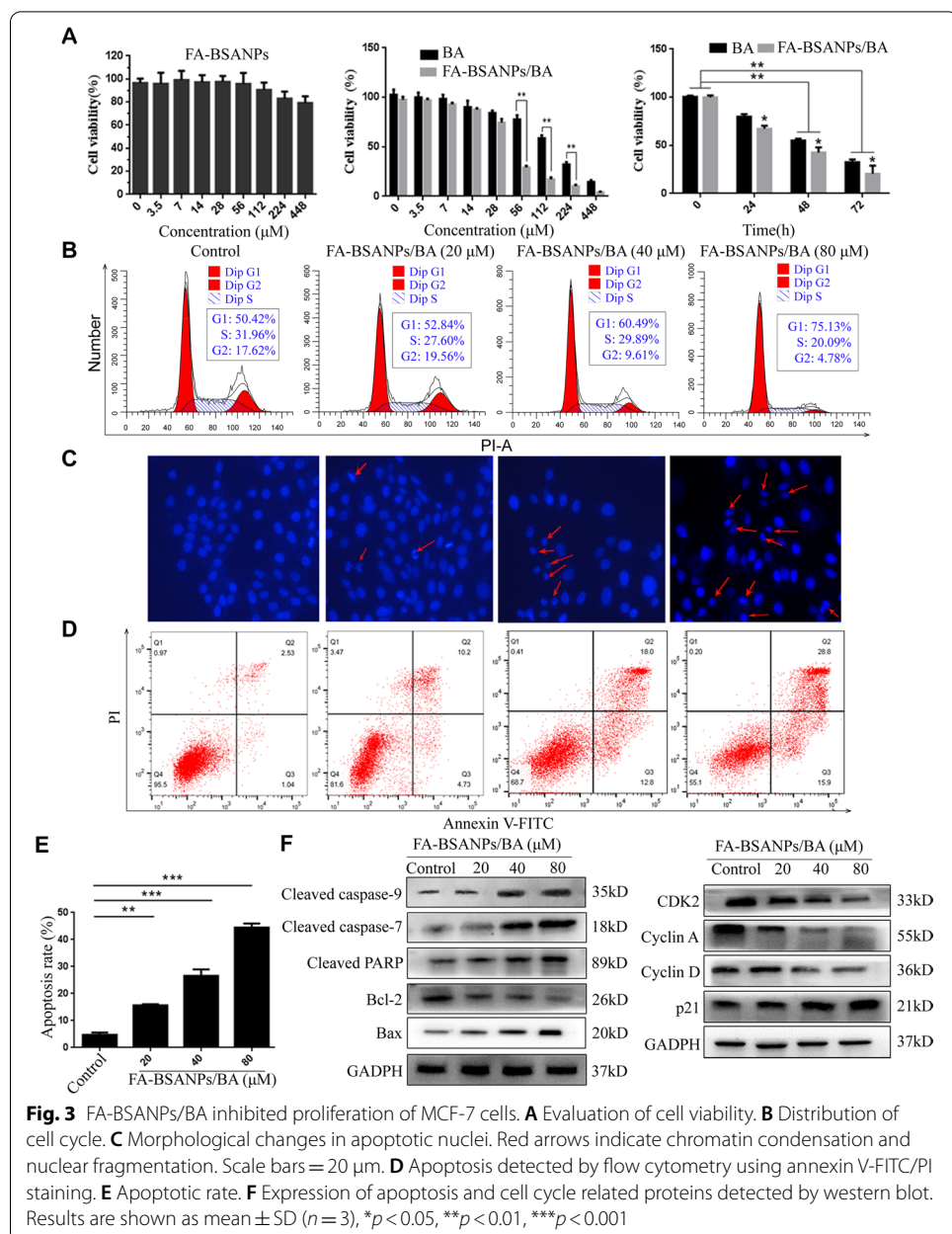


Fig. 3 FA-BSANPs/BA inhibited proliferation of MCF-7 cells. **A** Evaluation of cell viability. **B** Distribution of cell cycle. **C** Morphological changes in apoptotic nuclei. Red arrows indicate chromatin condensation and nuclear fragmentation. Scale bars = 20 μm . **D** Apoptosis detected by flow cytometry using annexin V-FITC/PI staining. **E** Apoptotic rate. **F** Expression of apoptosis and cell cycle related proteins detected by western blot. Results are shown as mean \pm SD ($n=3$), * $p<0.05$, ** $p<0.01$, *** $p<0.001$

medium, and high concentrations at 20, 40, 80 μM and a treatment time of 48 h were used for the next experiments.

Next, we evaluated the effects of FA-BSANPs/BA on cell cycle and apoptosis in MCF-7 cells. Compared with the control group, the percentage of G1-phase cell population was significantly increased after treatment with FA-BSANPs/BA for 48 h (Fig. 3B). Similarly, Western blot results showed that the expressions of CDK2, cyclin D and cyclin A were downregulated and the expression of p21 protein was upregulated in MCF-7 cells treated with FA-BSANPs/BA (Fig. 3F). Since chromatin condensation is one of the typical cell morphological changes in apoptotic cells, we stained MCF-7 cells with Hoechst 33342 and observed the morphological changes of the

cells. There were a large number of cells with intact round or oval nuclei and uniform staining in the control group, while in the FA-BSANPs/BA-treated cells appeared consolidated nuclei and dense blue fluorescent particles, which were formed apoptotic bodies (Fig. 3C).

AnnexinV-FITC/PI staining and flow cytometry analysis showed that the apoptosis rate of cells treated with FA-BSANPs/BA was significantly higher than that of the control group (Fig. 3D, E). Compared with the control group, FA-BSANPs/BA upregulated the expression of pro-apoptotic protein Bax and down regulated the expression of anti-apoptotic protein Bcl-2. In addition, compared with the control group, the expressions of cleaved caspase 9, 7 and PARP were also enhanced. These results indicated that FA-BSANPs/BA induced cell apoptosis mainly via mitochondria dependent intrinsic pathway (Fig. 3F). Our research evidence of cell cycle, apoptosis and viability is consistent with previous results (Gao et al. 2018). It was suggested that FA-BSANPs/BA could inhibit BC cell proliferation by inducing cell cycle arrest and apoptosis.

FA-BSANPs/BA induced autophagy in MCF-7 cells

Autophagy may serve as another mechanism leading to cell death. However, the dual role of autophagy both in cancer progression and inhibition remains controversial (Li et al. 2020). To determine whether FA-BSANPs/BA induce autophagy in BC cells and then participate in the mechanism of tumor suppression, we detected autophagic vesicles, which were specifically labeled using the CYTO-ID probe and colocalized with light chain 3 (LC3) in green to detect autophagosome formation, under autophagic flux (Xiang et al. 2020). As shown in Fig. 4A, cells treated with high concentration of FA-BSANPs/BA showed stronger green fluorescence compared with low concentration of FA-BSANPs/BA and control group. The results of Western blot showed that FA-BSANPs/BA upregulated LC3-II and Beclin-1 and down regulated LC3-I, which are important markers of autophagy process (Fig. 4B).

Next, we evaluated whether FA-BSANPs/BA-induced autophagy promotes or inhibits apoptosis in MCF-7 cells by pretreating with 2.5 mM 3-methyladenine (3-MA, an autophagy inhibitor) to illustrate the role of normal and nanoparticles induced autophagy in the growth of MCF-7. Figure 4C shows 3-MA increased the apoptosis rate of MCF-7 cells, indicating that autophagy is a protective mechanism in MCF-7 cells. The treatment of cells with FA-BSANPs/BA also increased the apoptosis rate, and the apoptosis induced by FA-BSANPs/BA decreased when combined with 3-MA, indicating that FA-BSANPs/BA-induced autophagy is harmful to MCF-7 cells, and autophagy is possibly the main mechanism of FA-BSANPs/BA inhibiting MCF-7 cells.

Apoptosis assay showed that 3-MA increased both apoptotic and necrotic cells, but the inhibition of apoptosis caused by FA-BSANPs/BA was not obvious when 3-MA and FA-BSANPs/BA were used in combination, while the necrotic cells were significantly decreased (Fig. 4D), which indicated that autophagy induced by FA-BSANPs/BA mainly caused type II cell death and less partially caused the cells to go the apoptotic program (type I cell death). This further confirmed that autophagy was the main mechanism of FA-BSANPs/BA inhibiting the growth of MCF-7 cells.

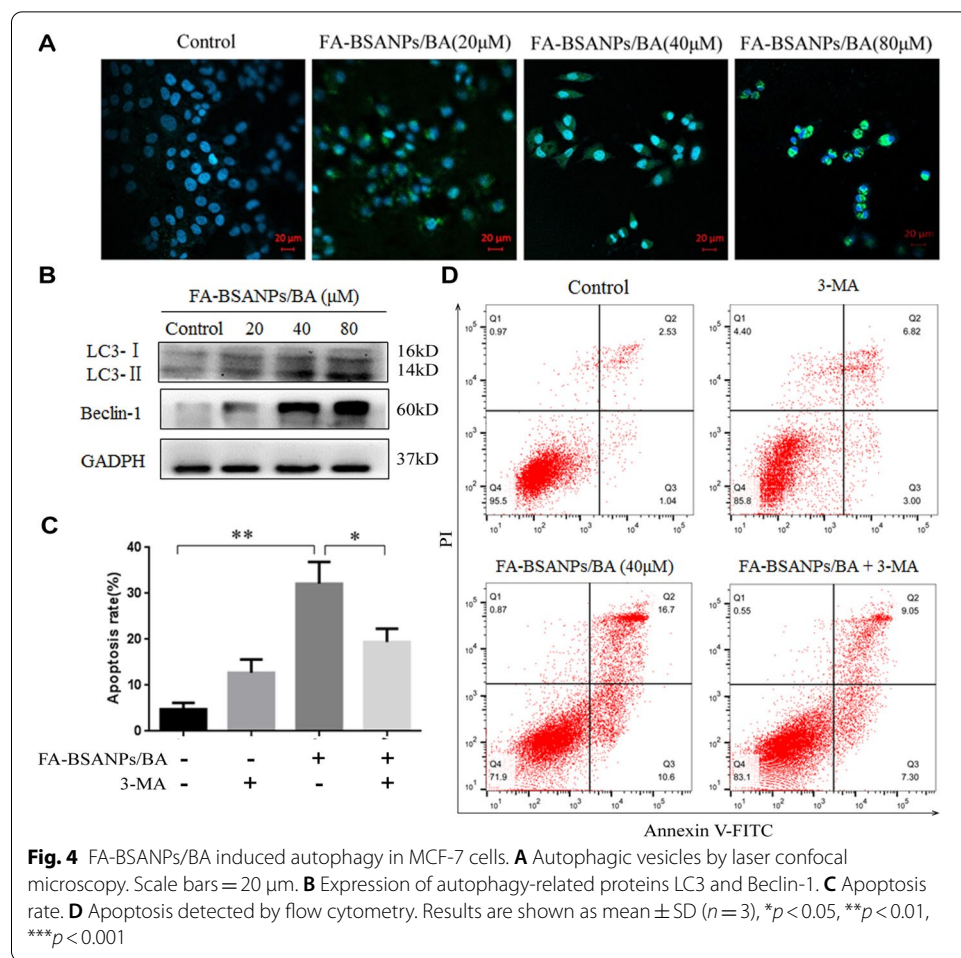


Fig. 4 FA-BSANPs/BA induced autophagy in MCF-7 cells. **A** Autophagic vesicles by laser confocal microscopy. Scale bars = 20 μ m. **B** Expression of autophagy-related proteins LC3 and Beclin-1. **C** Apoptosis rate. **D** Apoptosis detected by flow cytometry. Results are shown as mean \pm SD ($n=3$), * $p<0.05$, ** $p<0.01$, *** $p<0.001$

FA-BSANPs/BA regulated the phosphorylation of molecules in p38 MAPK and Akt/mTOR signaling pathways in MCF-7 cells

P38 MAPK and Akt/mTOR signaling pathways play important roles in physiological cellular activities such as proliferation, apoptosis, and autophagy (Wei et al. 2020). Generally, overactivation of p38 MAPK signaling is associated with enhanced autophagy, and Akt/mTOR signaling is an inhibitory mechanism of autophagy (Kim et al. 2017). Results showed that FA-BSANPs/BA led to downregulation of the protein expression of p38 MAPK, whereas the level of phosphorylated p38 MAPK was upregulated in a dose-dependent manner compared with the control group. FA-BSANPs/BA had no obvious effect on the protein expression of Akt, but led to a decrease in the protein expression of mTOR, and down regulated the levels of phosphorylated Akt and mTOR in a dose-dependent manner. In addition, pretreatment of samples with Akt inhibitor MK2206 and mTOR inhibitor rapamycin, respectively, decreased cell viability and increased pro-apoptotic proteins (Bax, PARP) and autophagy markers (LC3-II and Beclin-1) compared to the control group. And, there was an enhanced effect when MK2206 or rapamycin and FA-BSANPs/BA were combined. In contrast, cells pre incubated with p38 MAPK inhibitor SB203580 exhibited higher cell viability compared with the control group, and the effects of FA-BSANPs/BA were significantly reduced (Fig. 5). In conclusion, the

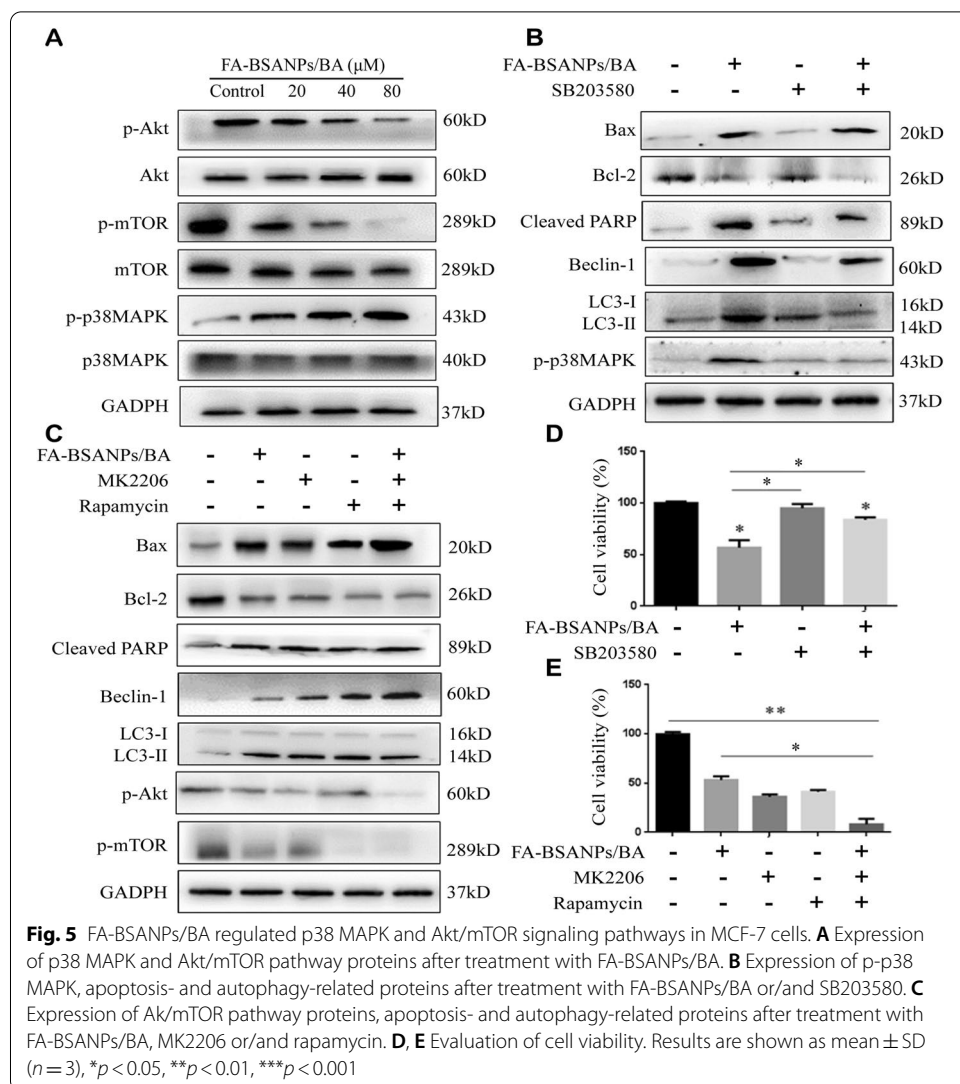


Fig. 5 FA-BSANPs/BA regulated p38 MAPK and Akt/mTOR signaling pathways in MCF-7 cells. **A** Expression of p38 MAPK and Akt/mTOR pathway proteins after treatment with FA-BSANPs/BA. **B** Expression of p-p38 MAPK, apoptosis- and autophagy-related proteins after treatment with FA-BSANPs/BA or/and SB203580. **C** Expression of Ak/mTOR pathway proteins, apoptosis- and autophagy-related proteins after treatment with FA-BSANPs/BA, MK2206 or/and rapamycin. **D, E** Evaluation of cell viability. Results are shown as mean \pm SD ($n=3$), * $p<0.05$, ** $p<0.01$, *** $p<0.001$

results of experiments using inhibitors demonstrated that p38 MAPK and Akt/mTOR signaling pathways are associated with autophagy and apoptosis in breast cancer MCF-7 cells. FA-BSANPs/BA exerted antiproliferative effects mainly by promoting phosphorylation of p38 MAPK and inhibiting phosphorylation of molecules in Akt/mTOR signaling pathway.

FA-BSANPs/BA increase the level of ROS in MCF-7 cells

ROS are known to be important regulators of p38 MAPK and Akt/mTOR signaling pathways and apoptosis and autophagy (Hung et al. 2016). Next, we further explored whether the upstream signals of the intervention mechanism of FA-BSANPs/BA in regulating p38 MAPK and Akt/mTOR signaling pathways involved ROS. As shown in Fig. 6A, the results showed that when cells were treated with FA-BSANPs/BA, the intracellular ROS level was significantly increased in all groups ($P<0.01$). It could be observed under a fluorescence microscope that cells treated with FA-BSANPs/BA (40 μ M) showed

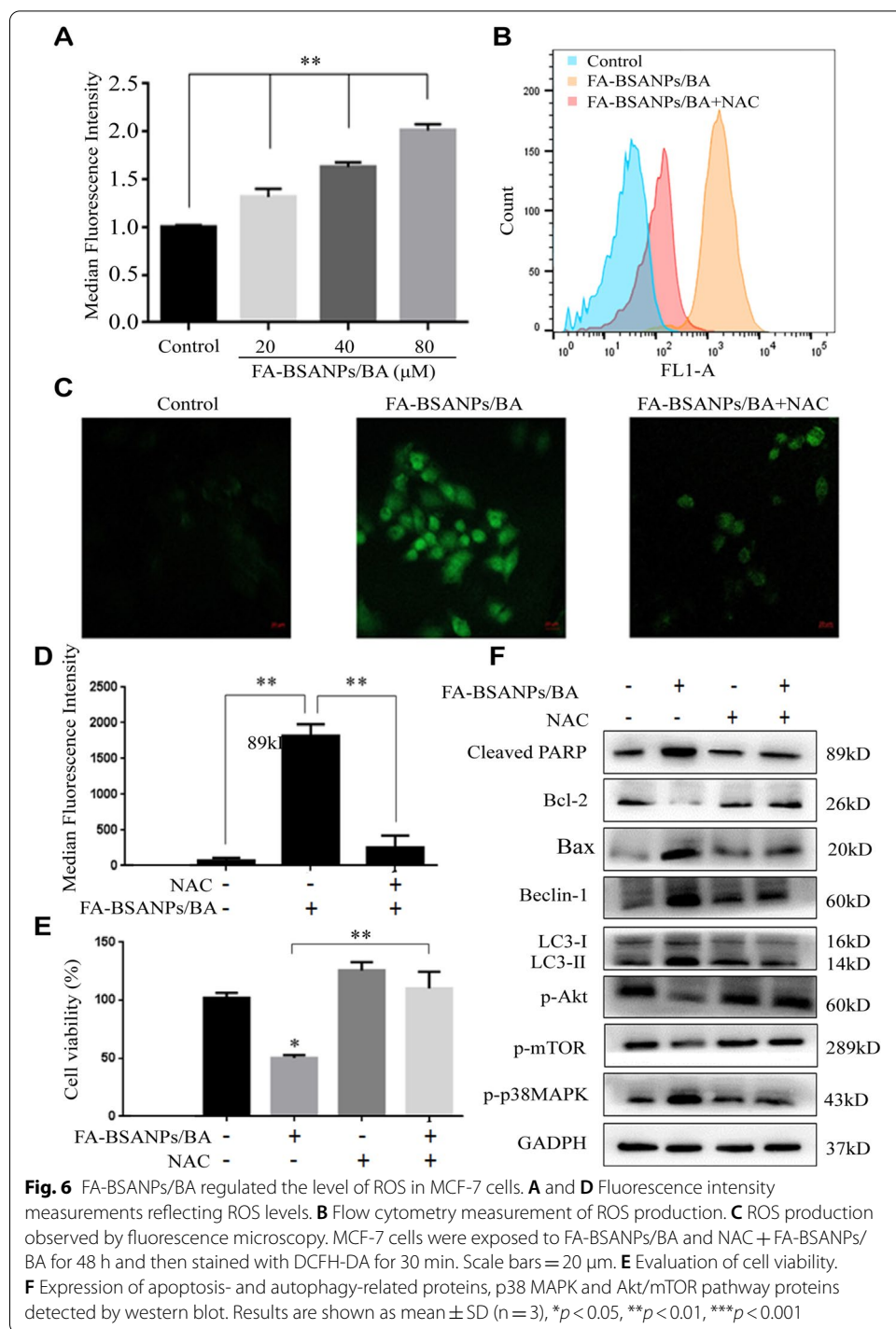


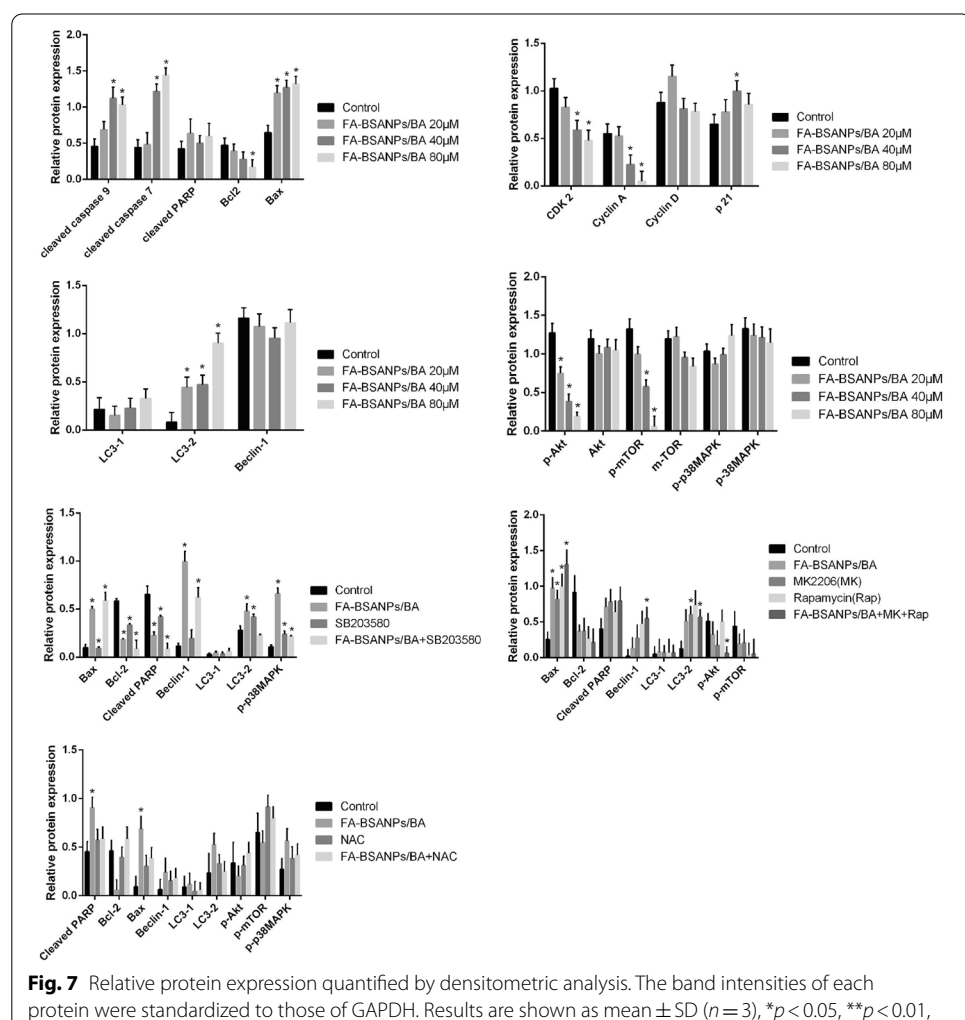
Fig. 6 FA-BSANPs/BA regulated the level of ROS in MCF-7 cells. **A** and **D** Fluorescence intensity measurements reflecting ROS levels. **B** Flow cytometry measurement of ROS production. **C** ROS production observed by fluorescence microscopy. MCF-7 cells were exposed to FA-BSANPs/BA and NAC + FA-BSANPs/BA for 48 h and then stained with DCFH-DA for 30 min. Scale bars = 20 μm . **E** Evaluation of cell viability. **F** Expression of apoptosis- and autophagy-related proteins, p38 MAPK and Akt/mTOR pathway proteins detected by western blot. Results are shown as mean \pm SD ($n=3$), * $p<0.05$, ** $p<0.01$, *** $p<0.001$

stronger green fluorescence than the control group (Fig. 6C). This was further confirmed by the fluorescence intensity of cells measured by flow cytometry (Fig. 6B). However, when the cells were pretreated with 5 mM N-acetylcysteine (NAC, a ROS scavenger), the promoting effect of FA-BSANPs/BA on ROS production was reversed (Fig. 6D), cell viability was reduced (Fig. 6E), and FA-BSANPs/BA induced increase in the expression

of pro-apoptotic proteins and autophagy markers was decreased, along with decreased p-p38 MAPK expression and upregulated p-Akt and p-mTOR expression (Fig. 6F). These results indicated that FA-BSANPs/BA regulated p38 MAPK and Akt/mTOR signaling pathways by increasing the level of ROS, and then inhibited the proliferation of BC cells. The quantitative results of all relative protein expression are shown in Fig. 7.

Discussion

The anti-BC potential of BA has been fully proved. In MCF-7 and MDA-MB-231 cells as well as in human BC xenograft mice, BA inhibited protein expression of NF- κ B-p65, increased NF- κ B-induced expression of CCND1, BCL2, BIRC2 and BIRC3, thereby inhibiting cell proliferation, invasion and migration, inducing G1/S phase cell cycle arrest and inhibiting anti-apoptotic factors in vitro and in vivo (Gao et al. 2018). BA could also inhibit BC cell survival, migration and invasion and promote apoptosis by regulating mir-338-3p and MORC4 (Duan et al. 2019). In addition, BA was reported to reverse the process of epithelial to mesenchymal transition (EMT) via inhibiting



TGF- β 1/p-Smad3 signaling and thus inhibit BC metastasis (Zhou et al. 2017; Liu et al. 2020). But there is no conclusive knowledge about the mechanism by which BA induces or inhibits autophagy in BC. And, the biggest problem of BA in cancer therapy is its poor water solubility.

Nanocarrier-based drug delivery systems show greater therapeutic potential in oncology, and modified nanocarrier platforms can improve drug bioavailability, reduce side effects, and enhance efficacy through targeted delivery and enhanced permeation effects. BA-loaded gold nanoparticles (AuNPs), PLGA nanocapsules and AuNPs conjugated with thiolated beta cyclodextrin (AuNP-S- β -CD) have been used to delivery BA to BC cells and found increased function (Singh et al. 2021; Lee et al. 2016). In this study, we prepared folic acid-modified bovine serum albumin nanoparticles encapsulating BA using a desolvation cross-linking technique. FA-BSANPs/BA showed spherical morphology and sustained-release behavior with appropriate encapsulation efficiency. Its sustained-release behavior was proven to be even more at lower pH conditions. Compared with normal tissues, some macromolecular substances with specific size (such as nanoparticles) are more likely to penetrate into tumor tissues and stay for a long time, which is called enhanced capability and retention effect (EPR). Based on this effect, the sustained-release behavior of FA-BSANPs/BA will be conducive to the aggregation of more BA at the tumor site and reduce the damage to normal cells. However, the use of the combination of sustained-release and tumor targeting may require more experimental data. More sophisticated design, such as the combination of pH-dependent preferential release in the microenvironment and tumor targeting, is a smarter strategy.

To evaluate targeting effect of the functional nanoparticles, we examined the uptake of tumor cells and macrophages in vitro. The intracellular median fluorescence intensity of FA-BSANPs/C6 group was significantly higher than that of BSANPs/C6 group and free C6 group. Free FA has been shown to hinder the uptake of FA-BSANPs/C6. When injected intravenously, because the particle size is in the range of 200 nm, the nanoparticles may be captured by the mononuclear phagocyte system first. Our results showed that the nanoparticles were indeed taken up by macrophages. Subsequent in vivo experiments also demonstrated drug accumulation in liver and kidney. It means that mononuclear phagocyte system could capture and remove some nanoparticles from the blood. However, the enrichment of nanoparticles at the tumor site was significantly more pronounced, which indicated that FA-conjugated BSA nanoparticles are good breast cancer targeting nanocarriers with potential for further improvement.

Subsequently, the antiproliferative activity of FA-BSANPs/BA was evaluated. Compared with free BA, FA-BSANPs/BA exhibited enhanced inhibitory effects on the viability of MCF-7 cells and could induce cell cycle arrest in G1-phase. However, future studies will be necessary to confirm the anticancer effect of FA-BSANPs/BA in other BC cell lines and in vivo. The current results will support our further optimization and modification of FA-BSANPs/BA.

Using folate albumin nanoparticles as carriers, we demonstrated that the mechanism of BA inhibiting BC proliferation was associated with regulation of autophagy and apoptosis, and autophagy is the main mechanism. Apoptosis activated by mitochondria-mediated intrinsic pathway is initiated by some signaling molecules. Cytochrome c is released from mitochondria into cytosol when the permeability of mitochondrial

membrane is altered. Upon receipt of an apoptotic signal, caspase-9 is activated first, followed by caspase-3, -6, and -7, ultimately leading to the cleavage of apoptosis related protein substrates (e.g., PARP), which is a process regulated by Bcl family proteins (Nagata 2018). Here, we found that FA-BSANPs/BA inhibited the expression of anti-apoptotic protein Bcl-2, elevated the expression of pro-apoptotic protein Bax, activated caspase-9, -7 in a dose-dependent manner, and subsequently caused shear inactivation of PARP, thereby inducing cell apoptosis.

It has been shown that BA was involved in the induction of autophagy in hepatoma cell line SMMC-7721 via autophagy-related proteins and Beclin-1 in a dose- and time-dependent manner (Zhang et al. 2012). We confirmed the production of autophagosomes and autophagy markers, autophagic vesicle formation, elevated Beclin-1 protein expression and conversion of LC3-I to LC3-II after FA-BSANPs/BA treatment by CYTO-ID green staining and immunoblot analysis, which indicated that FA-BSANPs/BA induced or promoted autophagy in MCF-7 cells. During tumor development, whether autophagy promotes survival or death has been a matter of debate. We found that pretreatment with autophagy inhibitor 3-MA could alleviate the toxicity of FA-BSANPs/BA on MCF-7 cells and the apoptotic rate of MCF-7 cells, which indicated that the autophagy induced by FA-BSANPs/BA in MCF-7 cells was detrimental to cell survival and might have promoted cell apoptosis and death.

However, as mentioned earlier, a key mechanism of autophagy promoting cancer is its ability to support cell metabolism. In some cancer types, the diverse metabolic fuels produced by autophagy provide metabolic plasticity for tumors and allow tumor cells to thrive in the harsh environment of hypoxia, low pH and nutrient deficiency (Kimmelman and White 2017). One limitation of this research is that all the experiments were completed in the presence of serum. Therefore, in the future study, it is necessary to study the significance of autophagy for BC cell survival and effect of BA and its nano-preparation on autophagy in a closer to the real situation of tumor models using anoxic environment, serum-free medium, acidic medium, co culture system or mouse models, in which the tumor cells may have a stronger malignant phenotype. Due to the relationship between autophagy and immunity, whether FA-BSANPs/BA-induced autophagy plays a role by activating antitumor immunity also needs further research. Furthermore, although autophagosome formation is one of the important pieces of evidence for the occurrence of autophagy, the detection of an integrated autophagic process including autophagosome formation, maturation, fusion with lysosomes and breakdown would provide a better explanation. Apoptosis and autophagy are complex processes regulated by multiple signaling pathways, including p38 MAPK and Akt/mTOR (Kim et al. 2017; Zhang et al. 2019). FA-BSANPs/BA could promote the phosphorylation of p38 MAPK and inhibit the phosphorylation of Akt and mTOR in MCF-7 cells, suggesting that the excessive apoptosis and autophagy induced by FA-BSANPs/BA may be associated with activating p38 MAPK and blocking Akt/mTOR signaling pathway. To further clarify the regulatory roles of p38 MAPK and mTOR pathways on FA-BSANPs/BA-induced apoptosis and autophagy, we pretreated cells with Akt inhibitor MK2206, mTOR inhibitor rapamycin and p38 MAPK inhibitor SB203580. The results showed that MK2206 and rapamycin significantly increased the expression of Beclin-1 and LC-3, activated Bax and PARP, and increased cell viability in MCF-7 cells. In addition, the expression levels of

apoptosis and autophagy-related proteins were decreased by SB203580, which reversed the antiproliferative activity of FA-BSANPs/BA. Collectively, these results indicated that apoptosis and autophagy induced by FA-BSANPs/BA were associated with p38 MAPK and Akt/mTOR pathways.

It has been reported that ROS are important regulators of many signal transduction pathways, and excessive ROS production leads to oxidative stress and activation of signaling pathways that regulate apoptosis and autophagy (Kaminskyy and Zhivotovsky 2014; Zou et al. 2017). In the present study, we found that exposure to FA-BSANPs/BA increased ROS production in MCF-7 cells, and resulted in altered p-p38 MAPK, p-Akt, p-mTOR activities and increased apoptosis and autophagy. This effect was further demonstrated using the ROS scavenger NAC. These results illustrated that ROS was the upstream factor of p38 MAPK activation and Akt/mTOR pathway inhibition, and the apoptosis and autophagy of BC cells induced by FA-BSANPs/BA might be associated with intracellular ROS accumulation.

Conclusion

FA-conjugated BSA nanoparticles are good carriers for BA and can effectively target breast tumor sites. Based on the present work, FA-BSANPs/BA exhibited more potent antiproliferation effects against breast cancer cells relative to BA, and this was achieved through the accumulation of ROS, which in turn caused the activation of p38 MAPK and the inhibition of Akt/mTOR signaling pathway, ultimately affecting the expression of cell cycle, apoptosis and autophagy-related proteins. Our findings provide potential candidates for the application of BA in BC therapy.

Materials and methods

Materials

BA (HPLC 98%, CAS#21,967–41-9, LOT: P20A9F59353) was provided by Shanghai yuanye Bio-Technology Co., Ltd (Shanghai, China); FA-BSANPs/BA is obtained from laboratory self-made. 3-Methyladenine (3-MA), SB203580, MK2206, rapamycin and N-AcetylL-cysteine (NAC) were purchased from Sigma-Aldrich (St. Louis, Missouri, USA). DMEM, phosphate buffered saline (PBS; pH = 7.4) and fetal bovine serum (FBS) were purchased from Gibco Life Technologies (New York, USA); MTT (3-(4,5-dimethylthiazol-2-yl)-2,5-diphenyltetrazolium bromide) Kit, Annexin V-FITC/PI apoptosis detection kit, 2,7-dichloro-dihydrofluorescein diacetate (DCFH-DA) and BCA Protein Assay Kit were acquired from Beyotime Biotechnology (Shanghai, China). The CYTO-ID autophagy detection kit was purchased from ENZO Life Sciences (NY, USA). Antibodies against cleaved caspase-9, cleaved caspase-7, cleaved PARP, Bax, Bcl-2, CDK2, Cyclin A, Cyclin D, p21, LC3, Beclin-1, phospho-Akt, Akt, phospho-mTOR, mTOR, phospho-p38 MAPK, p38 MAPK and GADPH were obtained from Cell Signaling Technology (Beverly, MA, USA).

Cell culture

The MCF-7 cell lines were obtained from Keygen Biotech (Nanjing, China) and cultured in DMEM medium (Gibco) with 10% fetal bovine serum and 1% 100 U/mL penicillin/streptomycin in a humidified incubator at 37 °C and 5% CO₂.

Animals

BALB/c female nude mice (18–22 g) obtained from Guangdong Medical Laboratory Animal Center were caged in specified pathogen free (SPF) animal room with an ambient temperature of 23 ± 2 °C, a relative humidity of $60 \pm 15\%$, light and shade of 12 h each, and fed freely. All the experimental procedures in this study were approved by the Animal experiment Center of Jinan University and followed the ethical principles of animal experiments. After 10 days of environmental adaptive culture, xenografts were first established as follows: MCF-7 cells (1×10^7 cells/mL) were mixed equivalently with matrigel and injected subcutaneously into the right forelimb armpit of BALB/c mice. The tumor model was considered successful when the tumor volume reached approximately 100 mm^3 .

Preparation and characterization of FA-BSANPs/BA

FA-BSANPs/BA were prepared using desolvation cross-linking technique as previously reported (Langer et al. 2003) (Meng et al. 2021). Briefly, Folate (FA), 1-ethyl-3-(3-dimethylaminopropyl) carbodiimide (EDC), N-hydroxysuccinimide (NHS) and 4-dimethylaminopyridine (DMAP) were added in dimethyl sulfoxide (DMSO) protected from light to activate FA by stirring at 50 °C. Bovine serum albumin was ultrasonic dissolved in buffer. The activation liquid of FA was added dropwise and allowed to react by slowly stirring in the dark at room temperature. Folate Modified Albumin Nanoparticles (FA-BSANPs) were obtained after the reaction was dialyzed against 10 mM/L NaHCO₃ and ultrapure water. BA was ultrasonic dissolved in an appropriate amount of absolute ethanol, adjusting pH 10 with NaOH and the oil–water ratio to 4:1 (v/v). A solution of absolute ethanol dissolved in BA was slowly dropped into FA-BSANPs dissolved in buffer under stirring condition at room temperature, and then 0.25% glutaraldehyde solution was added dropwise to solidify the crosslinks for 2 h. Finally, the solution was transferred into rotary evaporator to obtain FA-BSANPs/BA by rotary evaporation of ethanol solution at 37 °C, and then freeze-dried at 4 °C for sealed storage.

Transmission electron microscopy (TEM, TECNAI 10, Philips, Netherlands) was used to investigate the morphology of FA-BSANPs/BA. FTIR-8400 infrared spectrometer (Shimadzu, Japan) was used to analyze the preparation of sample flakes mixed with KBr. Particle size, polydispersity index (PDI) and zeta-potential were measured by Zetasizer Nano ZS90 (Malvern, UK). BA content in the nanoparticles was determined by high performance liquid chromatography (HPLC) (Agilent, USA). Ultraviolet (UV) spectrophotometry and BCA method were used to evaluate the conjugated amount of FA in FA-BSANPs/BA (Zhang et al. 2004).

In vitro drug release study

The release behavior of BA from FA-BSANPs/BA was determined by membrane dialysis method (Meng et al. 2021). Take 3 parts of 5 mL FA-BSANPs/BA solution with known concentration and put it into dialysis bag (MW 8000–14,000 kDa), then put the dialysis bag into phosphate buffered saline (PBS) with pH of 7.4, 6.5 and 5.5, respectively, and incubate it horizontally at 37.0 °C and 100 rpm. The release behavior of 5 mL BA solution in PBS at pH 7.4 was the control. To maintain sink conditions, 1% (V/V) polysorbate

80 (Tween 80) can be added to the acceptor phase. After dialysis for 1, 2, 4, 8, 12, 24, 36 and 48 h, 500 μ L release media were taken for analysis and replaced with fresh buffer. The samples were diluted with methanol and the content of BA was determined by HPLC. The experiment was repeated 3 times.

Qualitative and quantitative cellular uptake assays

The cellular uptake of the carrier systems in MCF-7 cells and Phorbol 12-myristate 13-acetate (PMA, 50 ng/mL for 3 days) induced macrophages (from human THP-1 cells) was explored using C6 and C6-labeled BSANPs and FA-BSANPs (Meng et al. 2021). Culture medium containing C6, BSANPs/ C6 and FA-BSANPs/ C6 (50 ng/mL, in terms of the concentration of C6), respectively, was added to the cells. After incubation for 4 h, Hoechst 33,342 (1:1000) was added to indicate cell nucleus and cultured for 10 min. The cellular uptake was observed under confocal microscope. Moreover, a flow cytometer (FACSCalibur, BD, USA) was used to determine the fluorescence intensity of the probes for cellular uptake quantification. Also, in order to examine the effect of folic acid in cellular uptake, control wells were set up to pretreat with folic acid for 1 h, followed by the addition of the same concentration of C6-FA-BSANPs.

Biodistribution assays

Either freely dissolved ICG or nanoparticles containing ICG were administered to the mice by tail vein injection at a dose of 2 mg/kg. The experiments were divided into ICG group, FA-BSA NPs/ICG group and dissection group with 6 mice in each group. Mice were anesthetized with 1% sodium pentobarbital (50 mg/kg, i.p.) before injection and at 0.5, 1, 4, 8, and 24 h after injection, and imaging analysis was performed using a small animal imaging system (IVIS lumina XR Series III, PerkinElmer, CA, USA). In addition, after 4 h of injection, the major organs (heart, liver, spleen, lung, kidney, and tumor tissue) of mice were removed for imaging analysis. Fluorescence intensities of whole body and tissue regions of mice were analyzed using IVIS lumina XR Series III software.

Cell viability assay

Cell viability was detected by MTT assay. 4×10^3 cells/well were seeded in 96-well plates and cultured in an incubator with 5% CO₂, 37 °C. After cell attachment, the original medium was replaced with fresh medium containing different concentrations (0, 3.5, 7, 14, 28, 56, 112, 224, 448 μ M) of FA-BSANPs, free BA or FA-BSANPs/BA and incubated for 24, 48 and 72 h. Cell viability was detected according to the instructions of the kit. The absorbance at 570 nm was detected using a microplate reader (Bio-Tek, USA).

Cell cycle analysis

5×10^5 cells/well were seeded in 6-well plates and cultured in an incubator with 5% CO₂, 37 °C. After cell attachment, the original medium was replaced with fresh medium containing different concentrations (0, 20, 40, 80 μ M) of FA-BSANPs/BA and incubated for 48 h. After collected and fixed overnight at – 20 °C in 75% ethanol, cells were stained with PI/RNase staining solution for 30 min at room temperature. Cell cycle was detected using flow cytometry (FACSCalibur, BD, USA) and analyzed using ModFit LT software.

Apoptotic cell morphology

5×10^4 cells/mL were seeded in 6-well plates and cultured in an incubator with 5% CO₂, 37 °C. After cell attachment, the original medium was replaced with fresh medium containing different concentrations of FA-BSANPs/BA for 48 h. After being washed twice with PBS, fixed with 4% paraformaldehyde solution for 20 min, and permeabilized with 0.1% Triton-X 100 for 10 min, cells were stained with Hoechst 33,342 solution (5 µg/mL) for 15 min in the dark at room temperature and then placed in a fluorescence microscope (Olympus, Tokyo, Japan) to observe cell morphology.

Flow cytometry analysis of apoptosis

Apoptosis detection was conducted using AnnexinV-FITC/PI apoptosis detection kit. Briefly, the cells were stained in 500 µL binding buffer containing 5 µL Annexin V-FITC and 5 µL PI in the dark at room temperature for 15 min. Apoptotic cells were analyzed by flow cytometry.

GFP-LC3 spot check

Cellular autophagy was assayed with the CYTO-ID Autophagy Assay Kit. 5×10^4 cells/mL were seeded in confocal dishes and cultured in an incubator with 5% CO₂, 37 °C. After cell attachment, the original medium was replaced with fresh medium containing different concentrations of FA-BSANPs/BA for 48 h. Cells were stained with CYTO-ID and Hoechst 33,342 solution, and then examined in a confocal microscope (Carl Zeiss LSM 510, Oberkochen, Germany) under which LC3-II was observed in a punctate form.

Intracellular ROS assay

The level of intracellular ROS was measured using 2,7-dichloro-dihydrofluorescein diacetate dye. 5×10^4 cells/mL were seeded in 6-well plates and cultured in an incubator with 5% CO₂, 37 °C. After attachment, cells were washed with PBS and stained with PBS containing 10 µM DCFH-DA for 30 min at 37 °C in the dark. ROS production was then measured on a confocal microscope and flow cytometer.

Western blot

5×10^5 cells/mL were seeded in 6-well plates and cultured in an incubator with 5% CO₂, 37 °C. After cell attachment, the original medium was replaced with fresh medium containing different concentrations of FA-BSANPs/BA for 48 h. Subsequently, samples were collected after lysis of cells with RIPA lysis buffer, and protein quantification was performed using the BCA kit. Protein samples were loaded onto 10% SDS-PAGE for separation and transferred to PVDF membranes, and after sealed with skimmed milk powder, membranes were incubated with rabbit primary antibody at 4 °C overnight. After washing with PBS, membranes were incubated with horseradish peroxidase-labeled secondary antibody, followed by the addition of ECL luminescent solution in the dark and imaged with an imaging system (Tanon-5200Multi, Shanghai, China). The bands were quantified by scanning of the radiographic films

followed by estimation of the density and area of the bands using ImageJ JS software (<https://ij.imjoy.io/>). Data of relative protein expression in this study are shown in Fig. 6.

Statistical analysis

Statistical analysis was performed using GraphPad Prism 6.0. All experimental data were expressed as mean \pm SD in triplicate. Subgroup differences among different experimental and control groups were assessed using Student's t-test or analysis of variance (ANOVA) with Bonferroni adjustment for multiple comparison. Statistical significance was identified as $*p < 0.05$, $**p < 0.01$, $***p < 0.001$.

Supplementary Information

The online version contains supplementary material available at <https://doi.org/10.1186/s12645-021-00110-x>.

Additional file 1: Fig. S1. Near-infrared fluorescence imaging (The figure was quoted from reference (Meng et al. 2021), and we have obtained permission from the copyright holder to reproduce it). **A** ICG group. **B** FA-BSANPs/ ICG group. In each group, the upper part shows representative images of MCF-7 tumor-bearing mice before injection and at 0.5, 1, 4, 8, and 24 h after injection, and the lower part shows representative images of tumor tissue, heart, liver, spleen, lung and kidney at 4 h after injection. ICG indocyanine green.

Acknowledgements

Not applicable.

Authors' contributions

FL, ML and BR made substantial contributions to the design of the work, the acquisition, analysis, and interpretation of data and the writing of the work; LL prepared the FA-BSANPs/BA for in vitro experiments; TZ participated in the autophagy-related experiments; ZK participated in the Western blot experiments; ZY, TC and YC revised the manuscript. All authors read and approved the final manuscript.

Funding

This work was supported by the [Projects of International Cooperation and Exchanges of National Natural Science Foundation of China #1] under Grant [Number 82020108033]; and [Natural Science Foundation of Guangdong #2] under Grant [Number 2019A1515011286].

Availability of data and materials

Data generated or analyzed during this study are included in this published article [and in Additional file 1].

Declarations

Ethics approval and consent to participate

Not applicable.

Consent for publication

Not applicable.

Competing interests

The authors declare that they have no competing interests.

Author details

¹College of Pharmacy, Jinan University, Guangzhou 510632, Guangdong, China. ²Medical Department of Guangdong Hospital of Traditional Chinese Medicine, Guangzhou 510405, Guangdong, China. ³Department of Gastroenterology, First Affiliated Hospital of Guangzhou University of Chinese Medicine, Guangzhou 510405, Guangdong, China. ⁴College of Life Sciences, Liaoning University, Shenyang 110036, Liaoning, China. ⁵Guangdong Key Lab of Traditional Chinese Medicine Information Technology, Jinan University, Guangzhou 510632, Guangdong, China.

Received: 24 June 2021 Accepted: 3 December 2021

Published online: 06 January 2022

References

Ahmed IS, Rashed HM, Fayed H, Farouk F, Shamma RN (2020) Nanoparticle-mediated dual targeting: an approach for enhanced baicalin delivery to the liver. *Pharmaceutics*. <https://doi.org/10.3390/pharmaceutics1220107>

- Bhushan B, Khanadeev V, Khlebtsov B, Khlebtsov N, Gopinath P (2017) Impact of albumin based approaches in nanomedicine: imaging, targeting and drug delivery. *Adv Colloid Interface Sci* 246:13–39
- Carneiro BA, El-Deyri WS (2020) Targeting apoptosis in cancer therapy. *Nat Rev Clin Oncol* 17(7):395–417
- De Cicco P, Catani MV, Gasperi V, Sibilano M, Quaglietta M, Savini I (2019) Nutrition and breast cancer: a literature review on prevention, treatment and recurrence. *Nutrients*. <https://doi.org/10.3390/nu11071514>
- Duan X, Guo G, Pei X, Wang X, Li L, Xiong Y et al (2019) Baicalin inhibits cell viability, migration and invasion in breast cancer by regulating miR-338-3p and MORN4. *Oncotargets Ther* 12:11183–11193
- Gao C, Zhou Y, Li H, Cong X, Jiang Z, Wang X et al (2017) Antitumor effects of baicalin on ovarian cancer cells through induction of cell apoptosis and inhibition of cell migration in vitro. *Mol Med Rep* 16(6):8729–8734
- Gao Y, Liu H, Wang H, Hu H, He H, Gu N et al (2018) Baicalin inhibits breast cancer development via inhibiting IκB kinase activation in vitro and in vivo. *Int J Oncol* 53(6):2727–2736
- Hung Y-C, Pan T-L, Hu W-L (2016) Roles of reactive oxygen species in anticancer therapy with *Salvia miltiorrhiza* bunge. *Oxid Med Cell Longev* 2016:5293284
- Kaminsky VO, Zhivotovsky B (2014) Free radicals in cross talk between autophagy and apoptosis. *Antioxid Redox Signal* 21(1):86–102
- Kim K-Y, Park K-I, Kim S-H, Yu S-N, Park S-G, Kim YW et al (2017) Inhibition of Autophagy promotes salinomycin-induced apoptosis via reactive oxygen species-mediated PI3K/AKT/mTOR and ERK/p38 MAPK-dependent signaling in human prostate cancer cells. *Int J Mol Sci*. <https://doi.org/10.3390/ijms18051088>
- Kimmelman AC, White E (2017) Autophagy and tumor metabolism. *Cell Metab* 25(5):1037–1043
- Langer K, Balthasar S, Vogel V, Dinauer N, von Briesen H, Schubert D (2003) Optimization of the preparation process for human serum albumin (HSA) nanoparticles. *Int J Pharm* 257(1–2):169–180
- Lee D, Ko W-K, Hwang D-S, Heo DN, Lee SJ, Heo M et al (2016) Use of baicalin-conjugated gold nanoparticles for apoptotic induction of breast cancer cells. *Nanoscale Res Lett* 11(1):381
- Li X, He S, Ma B (2020) Autophagy and autopagy-related proteins in cancer. *Mol Cancer* 19(1):12
- Lian B, Wu M, Feng Z, Deng Y, Zhong C, Zhao X (2019) Folate-conjugated human serum albumin-encapsulated resveratrol nanoparticles: preparation, characterization, bioavailability and targeting of liver tumors. *Artif Cells Nanomed Biotechnol* 47(1):154–165
- Liu D-K, Dong H-F, Liu R-F, Xiao X-L (2020) Baicalin inhibits the TGF-β1/p-Smad3 pathway to suppress epithelial-mesenchymal transition-induced metastasis in breast cancer. *Oncotarget* 11(29):2863–2872
- Li-Weber M (2009) New therapeutic aspects of flavones: the anticancer properties of Scutellaria and its main active constituents Wogonin, Baicalein and Baicalin. *Cancer Treat Rev* 35(1):57–68
- Mancias JD, Kimmelman AC (2016) Mechanisms of selective autophagy in normal physiology and cancer. *J Mol Biol* 428:1659–1680
- Meng F, Liu F, Lan M, Zou T, Li L, Cai T et al (2021) Preparation and evaluation of folate-modified albumin baicalin-loaded nanoparticles for the targeted treatment of breast cancer. *J Drug Deliv Sci Technol* 65:102603
- Moloney JN, Cotter TG (2018) ROS signalling in the biology of cancer. *Semin Cell Dev Biol* 80:50–64
- Nagata S (2018) Apoptosis and clearance of apoptotic cells. *Annu Rev Immunol* 36:489–517
- Peng Y, Fu Z-Z, Guo C-S, Zhang Y-X, Di Y, Jiang B et al (2015) Effects and mechanism of baicalin on apoptosis of cervical cancer hela cells in-vitro. *Iran J Pharm Res* 14(1):251–261
- Prasad S, Gupta SC, Tyagi AK (2017) Reactive oxygen species (ROS) and cancer: Role of antioxidative nutraceuticals. *Cancer Lett Ireland* 387:95–105
- Shen Z, Li Y, Kohama K, Oneill B, Bi J (2011) Improved drug targeting of cancer cells by utilizing actively targetable folic acid-conjugated albumin nanospheres. *Pharmacol Res* 63(1):51–58
- Siegel RL, Miller KD, Jemal A (2020) Cancer statistics, 2020. *CA Cancer J Clin* 70(1):7–30
- Singh S, Meena A, Luqman S (2021) Baicalin mediated regulation of key signaling pathways in cancer. *Pharmacol Res* 164:105387
- Sui X, Kong N, Ye L, Han W, Zhou J, Zhang Q et al (2014) p38 and JNK MAPK pathways control the balance of apoptosis and autophagy in response to chemotherapeutic agents. *Cancer Lett* 344(2):174–179
- Tao C, Chuah YJ, Xu C, Wang D-A (2019) Albumin conjugates and assemblies as versatile bio-functional additives and carriers for biomedical applications. *J Mater Chem B* 7(3):357–367
- Trachootham D, Alexandre J, Huang P (2009) Targeting cancer cells by ROS-mediated mechanisms: a radical therapeutic approach? *Nat Rev Drug Discov* 8(7):579–591
- Waks AG, Winer EP (2019) Breast cancer treatment: a review. *JAMA* 321(3):288–300
- Wei T, Xiaojun X, Peilong C (2020) Magnoflorine improves sensitivity to doxorubicin (DOX) of breast cancer cells via inducing apoptosis and autophagy through AKT/mTOR and p38 signaling pathways. *Biomed Pharmacother* 121:109139
- Xiang W, Zhang R-J, Jin G-L, Tian L, Cheng F, Wang J-Z et al (2020) RCE-4, a potential anti-cervical cancer drug isolated from Reineckia carnea, induces autophagy via the dual blockade of PI3K and ERK pathways in cervical cancer CaSkI cells. *Int J Mol Med* 45(1):245–254
- Yang S, Lian G (2020) ROS and diseases: role in metabolism and energy supply. *Mol Cell Biochem* 467(1–2):1–12
- Zhang L, Hou S, Mao S, Wei D, Song X, Lu Y (2004) Uptake of folate-conjugated albumin nanoparticles to the SKOV3 cells. *Int J Pharm* 287(1–2):155–162
- Zhang L, Hou S, Zhang J, Hu W, Wang C (2010) Preparation, characterization, and in vivo evaluation of mitoxantrone-loaded, folate-conjugated albumin nanoparticles. *Arch Pharm Res* 33(8):1193–1198
- Zhang X, Tang X, Liu H, Li L, Hou Q, Gao J (2012) Autophagy induced by baicalin involves downregulation of CD147 in SMMC-7721 cells in vitro. *Oncol Rep* 27(4):1128–1134
- Zhang G, He J, Ye X, Zhu J, Hu X, Shen M et al (2019) β-Thujaplicin induces autophagic cell death, apoptosis, and cell cycle arrest through ROS-mediated Akt and p38/ERK MAPK signaling in human hepatocellular carcinoma. *Cell Death Dis* 10(4):255
- Zhao D, Zhao X, Zu Y, Li J, Zhang Y, Jiang R et al (2010) Preparation, characterization, and in vitro targeted delivery of folate-decorated paclitaxel-loaded bovine serum albumin nanoparticles. *Int J Nanomedicine* 5:669–677

- Zhou Q, Wang S, Zhang H, Lu Y, Wang X, Motoo Y et al (2009) The combination of baicalin and baicalein enhances apoptosis via the ERK/p38 MAPK pathway in human breast cancer cells. *Acta Pharmacol Sin* 30(12):1648–1658
- Zhou T, Zhang A, Kuang G, Gong X, Jiang R, Lin D et al (2017) Baicalin inhibits the metastasis of highly aggressive breast cancer cells by reversing epithelial-to-mesenchymal transition by targeting β-catenin signaling. *Oncol Rep* 38(6):3599–3607
- Zhu Y, Fang J, Wang H, Fei M, Tang T, Liu K et al (2018) Baicalin suppresses proliferation, migration, and invasion in human glioblastoma cells via Ca(2+)-dependent pathway. *Drug Des Devel Ther* 12:3247–3261
- Zou Z, Chang H, Li H, Wang S (2017) Induction of reactive oxygen species: an emerging approach for cancer therapy. *Apoptosis* 22(11):1321–1335

Publisher's Note

Springer Nature remains neutral with regard to jurisdictional claims in published maps and institutional affiliations.

Ready to submit your research? Choose BMC and benefit from:

- fast, convenient online submission
- thorough peer review by experienced researchers in your field
- rapid publication on acceptance
- support for research data, including large and complex data types
- gold Open Access which fosters wider collaboration and increased citations
- maximum visibility for your research: over 100M website views per year

At BMC, research is always in progress.

Learn more biomedcentral.com/submissions

